GRANULAR FLOW SIMULATIONS OF LIMITING REGIMES OF PARTICLES–WALL INTERACTION RELEVANT TO SLAGGING COAL GASIFIERS

Andrea Aprovitola [a], Francesco Saverio Marra [b],
Fabio Montagnaro [c], Piero Salatino [d]

[a] *Istituto di Calcolo e Reti ad Alte Prestazioni, CNR, Via Pietro Castellino 111, 80131 Napoli, Italy*
Email: andrea.aprovitola@na.icar.cnr.it
[b] *Istituto di Ricerche sulla Combustione, CNR, Via Diocleziano 328, 80124 Napoli, Italy.*
Email: marra@irc.cnr.it
[c] *Dipartimento di Scienze Chimiche, Università degli Studi di Napoli Federico II, Complesso Universitario di Monte Sant'Angelo, 80126 Napoli, Italy.*
Email: fabio.montagnaro@unina.it
[c] *Dipartimento di Ingegneria Chimica, dei Materiali e della Produzione Industriale, Università degli Studi di Napoli Federico II, Piazzale Tecchio 80, 80125 Napoli, Italy.*
Email: piero.salatino@unina.it

ABSTRACT

In pilot entrained-flow slagging coal gasifiers, high conversion efficiency and low pollutant emission levels have been observed, but the mechanism leading to this behaviour is not fully understood. Recent literature proposes several different mechanisms as playing an important role, ranging from the sticking properties of both particles and slag-covered walls to the thermal and chemical history along the trajectory of the particles in the entire gasifier. Nonetheless, very few attention has been devoted to the role of particle–particle interactions, even if it has been shown that this mechanism can lead to new regimes likely to occur in slagging gasifiers and to promote the rise in the coal conversion efficiency.

This study presents the results of a simplified configuration that allows to highlight the role of the four different interactions that can be envisaged when considering particles and confining walls as either sticky or non sticky. Particles are subjected to a body force that mimics the action of the drag exerted by a swirling flow field in a cylindrical vessel. Particle–particle collisions are modelled with an Hertzian approach that includes torque and cohesion effects. Results clearly indicate the different structure of the layer of particles establishing on the wall surface in the different interaction regimes. They confirm the importance to adequately take into account particle–particle interactions for a correct prevision of the fate of coal particles in slagging gasifiers.

1. INTRODUCTION

Combustion/gasification under slagging conditions are key aspects of the design of modern entrained-flow reactors for thermal conversion of solid fuels, to increase the overall energy efficiency [1,2]. Understanding the phenomenology and proper design of slagging entrained-flow reactors requires the assessment of the fate of char particles as they impinge on the wall

slag layer [3,4]. In previous theoretical and experimental studies of this research group [5–8], it was developed a phenomenological model that considers the establishment of a particle segregated phase in the near-wall region of the gasifier. In fact, it was highlighted that char particles impinging on the wall slag layer can either be entrapped inside the melt (a condition that hampers further progress of combustion/gasification), or adhere onto the slag layer's surface (progress of combustion/gasification is still possible in this case). In the latter case, and if the slag layer is extensively covered by char particles, a particle segregated phase may establish in the close proximity of the wall ash layer, where the excess impinging char particles that cannot be accommodated on the slag surface accumulate. This annular phase is slower than the lean particle-laden gas phase (that characterizes the entrained flow), so that the residence times of char particles are longer than the average gas space-time, with a positive impact on carbon burn-off. In a recent paper [9], with the aim of improving the mechanistic understanding of particle–wall interactions in entrained-flow systems, the authors used the tool of physical modeling: particle–wall interactions were investigated in a lab-scale cold entrained-flow reactor, equipped with a nozzle whence molten wax is atomized into a mainstream of air.

It is known that different micromechanical char–slag interaction patterns may establish, depending on the particle and the wall temperatures, on the solid/molten status of the particles impinging the slag layer or making up the slag itself, on the char conversion degree, on the particle kinetic energy, on the surface tension. Four different patterns are envisaged on the basis of the "stickiness degree" of the wall layer and of the impinging char particle [9]: *(i)* sticky particle (SP) impinging on a sticky wall (SW); *(ii)* non sticky particle (NSP) impinging on a sticky wall; *(iii)* sticky particle impinging on a non sticky wall (NSW); *(iv)* non sticky particle impinging on a non sticky wall. In this paper, SP is represented by partially molten particles and NSP by perfectly rigid, cold particles; on the other hand, SW is represented by walls covered by molten slag and NSW by uncovered walls or by walls covered by a slag layer itself covered by char particles.

This paper lays along the path set by the authors in previous modelling works [5–8]. Aim of the simulations of this paper is to represent, in the most simplified way, the effective mechanism of interaction of a flux of particles that reaches a cylindrical wall under the effect of volume forces. Here, these forces represent a very crude model for the action of a swirled flow dragging the particles. Objective of the simulations is to investigate the structure of the forming layer near the wall and to establish conditions leading to equilibrium for particles, wall and interaction parameters likely to reproduce, under conditions representative of carbon and ash particles in entrained-flow reactors, the four limiting regimes previously listed.

2. MODELLING APPROACH

Particles motion is described in the framework of the Discrete Element Method (DEM) based on the soft sphere approach proposed by Cundall and Strack [10]. Such choice is here motivated by the finding that, under typical conditions of entrained-flow gasifiers, a large number of particles starts to accumulate very soon near the confining walls [7]. Therefore, the model aims to represent conditions characterized by high particle concentrations, as those expected to occur as a consequence of the "segregation–coverage" regime [5], where the collisions of multiple particles make their mutual interaction predominant with respect to the action of the bulk gas phase.

Interparticle contact is modelled as a spring–dashpot system, that accounts for both oblique collisions and damping. Following Cundall and Strack [10], the model relates the normal

contact force exerted between two particles during an elastic collision to their deformation history. Adopting the nomenclature illustrated in Fig. 1, the particles contact force is decomposed into a normal and a tangential force, $\mathbf{F}_{c,ij} = \mathbf{F}_{n,ij} + \mathbf{F}_{t,ij}$, whose expressions are respectively:

$$\mathbf{F}_{n,ij} = -k_{n,ij}\mathbf{d}_{n,ij} - \gamma_{n,ij}\mathbf{v}_{n,ij} \tag{1}$$

$$\mathbf{F}_{t,ij} = -k_{t,ij}\mathbf{d}_{t,ij} - \gamma_{t,ij}\mathbf{v}_{t,ij} \tag{2}$$

where $d = R_\mathrm{i} + R_\mathrm{j}$, $d_{n,ij} = d_{ij} - \delta_{n,ij}$. $\mathbf{d}_{n,ij}$ and $\mathbf{d}_{t,ij}$ in Eqs. (1) and (2) are respectively the normal and tangential displacement vector between two spherical particles i and j, $k_{n,ij}$ and $k_{t,ij}$ the normal and the tangential stiffness, $\gamma_{n,ij}$ and $\gamma_{t,ij}$ the viscoelastic damping constant for normal and tangential contact, $\mathbf{v}_n$ and $\mathbf{v}_t$ the normal and tangential component of the relative velocity of the particle upon contact. Both normal contact and tangential contact forces have two contributions. The meaning of the contribution of the normal component has been explained, while the two contributions of the tangential contact force are the shear force and the damping force. The shear force is an history effect that accounts for the tangential displacement (tangential overlap) between the particles for the duration of the time they are in contact. If the magnitude of the tangential component is $|\mathbf{F}_{t,ij}| < \mu |\mathbf{F}_{n,ij}|$ where μ is the static friction coefficient, the contact is retained, otherwise the particles will slide on each other. The translational motion of the particle i is described by:

$$m_i \frac{d\mathbf{u}_i}{dt} = \sum_{j=1}^{n_p} (\mathbf{F}_{n,ij} + \mathbf{F}_{t,ij}) \tag{3}$$

representing m_i, $\mathbf{u}_i$, n_p, $\mathbf{F}_{n,ij}$, $\mathbf{F}_{t,ij}$, the particle mass, velocity, number of particles, normal interparticle contact force (elastic + viscous) and tangential interparticle contact force (elastic + viscous), respectively. The rotational motion of the particle i is described by:

$$I_i \frac{d\boldsymbol{\omega}_i}{dt} = \sum_{j=1}^{n_p} (\mathbf{T}_{t,ij} + \mathbf{T}_{r,ij}) \tag{4}$$

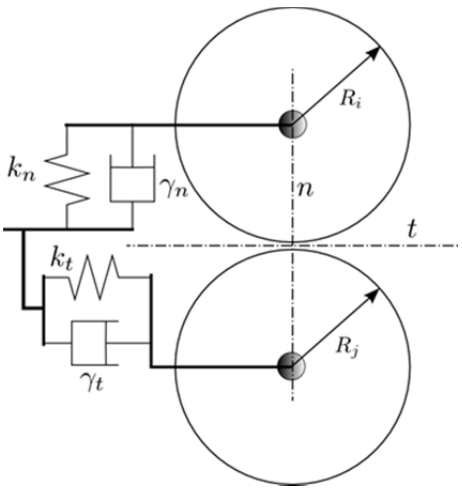

Figure 1. Spring–dashpot contact model.

being I_i, $\boldsymbol{\omega}_i$, the moment of inertia and the rotational velocity of the particle *i*, respectively, while $\mathbf{T}_{t,ij}$ is the tangential torque and $\mathbf{T}_{r,ij} = \mu_r |\mathbf{F}_n| \frac{\boldsymbol{\omega}_{r,ij}}{|\boldsymbol{\omega}_{r,ij}|} R_p$ the rolling friction torque, where $\boldsymbol{\omega}_{r,ij}$ is the relative rotational velocity between two particles [11], μ_r is the nondimensional rolling friction coefficient and R_p the particle radius. It is worth to remark that in all the results presented here, the contribution due to the rolling friction among particle–particle interactions is not taken into account, while it is accounted for particle–wall interactions.

In the soft sphere approach, the behaviour of a granular material is characterized by the mechanical properties of the particle material [12] (i.e. density ρ, Young's modulus Y, Poisson's ratio ν and shear modulus G). If $\delta_{n,ij}$ is the particles overlap, or deformation, the coefficients of Eqs. (1) and (2) are given by:

$$k_{n,ij} = \frac{4}{3} Y^* \sqrt{R^* \delta_{n,ij}}\,, \quad \gamma_{n,ij} = -2\sqrt{\frac{5}{6}}\beta\sqrt{S_n m^*}\,, \quad k_{t,ij} = 8G^*\sqrt{R^*\delta_{n,ij}}\,, \quad \gamma_{t,ij} = -2\sqrt{\frac{5}{6}}\beta\sqrt{S_t m^*} \tag{5}$$

In these equations:

$$S_n = 2Y^*\sqrt{R^*\delta_{n,ij}} \quad , \quad S_t = 8G^*\sqrt{R^*\delta_{n,ij}} \quad , \quad \beta = \frac{\ln\varepsilon}{\sqrt{\ln^2\varepsilon + \pi^2}} \tag{6}$$

where starred parameters indicate the equivalent values of Young's modulus, shear modulus, radius and mass, respectively, for the system of interacting particles *i* and *j*, and ε is the restitution coefficient:

$$\frac{1}{Y^*} = \frac{1-\nu_i^2}{Y_i} + \frac{1-\nu_j^2}{Y_j}\,, \quad \frac{1}{G^*} = \frac{2(2+\nu_i)(1-\nu_i)}{Y_i} + \frac{2(2+\nu_j)(1-\nu_j)}{Y_j} \tag{7}$$

$$\frac{1}{R^*} = \frac{1}{R_i} + \frac{1}{R_j}\,, \qquad \frac{1}{m^*} = \frac{1}{m_i} + \frac{1}{m_j} \tag{8}$$

In granular flows, the capability to transmit tangential forces among particles without the presence of a normal force is accounted by cohesion. The cohesion force can be computed with a linear model, linking the magnitude of the force to the particle contact surface area, $\mathbf{F}_{cohesion} = cA\mathbf{n}$, where c is the value of the cohesion energy density, A is the contact surface among the particles considered as plane disks and $\mathbf{n}$ is the unit vector normal to particle surface contact areas. If $R_i = R_j = R_p$, it is computed as:

$$A = \frac{\pi}{4}\left[R_p^2 - \left(R_p - \delta_n\right)^2\right] \tag{9}$$

This model and a very efficient integration procedure is available in the LIGGGHTS code [13], here adopted to obtain all the presented simulation results.

3. CASE GEOMETRY AND SETUP

The simulations have been performed setting the particles radius R_p = 100 μm, having density ρ = 1100 kg/m^3. The mechanical properties are those of pulverized coal and are reported in Table 1 [14]. The cohesion energy density is c = 100000 N/m^2 for all the interactions

considered. An initial bunch of n_p = 60500 particles, assumed to be spherical, is initially deposited in the core of a cylindrical region with the axis of the cylinder coincident with the z-axis, centred around the point having coordinates (0, 0) in the xy plane, and with upper and lower basis located at z = 0 and z = 0.01 m. The total number of particles is chosen as those corresponding to the number of particles disposable in a perfect packing to form two layers of particles that completely cover the walls. The radius of the insertion cylinder is chosen as $R_{ins} > \left[\left(4 n_p R_p^3\right)/\left(\alpha_p h_{ins}\right)\right]^{1/2}$, being $\alpha_p = V_p n_p / V_{ins} = 0.5$ the particle volume fraction and h_{ins} = 0.01 m the cylinder height, respectively. This leads the radius to be R_{ins} = 0.005 m.

Table 1: particle–wall mechanical properties.

Regime	ρ [kg/m^3]	Y [GPa]	ν [–]	$\varepsilon_{i,j}$ [–]	$\mu_{i,j}$ [–]	$\mu_{r_{i,j}}$ [–]
NSP–NSW	1100	3	0.37	0.9, 0.9, 0.9, 0.9	0.3, 0.3, 0.3, 0.3	0.3, 0.3, 0.3, 0.3
NSP–SW	1100	3	0.37	0.9, 0.1, 0.1, 0.1	0.3, 5e3, 5e3, 5e3	0.3, 5e3, 5e3, 5e3
SP–NSW	1100	3	0.37	0.1, 0.9, 0.9, 0.9	5e3, 0.3, 0.3, 0.3	5e3, 0.3, 0.3, 0.3
SP–SW	1100	3	0.37	0.1, 0.1, 0.1, 0.1	5e3, 5e3, 5e3, 5e3	5e3, 5e3, 5e3, 5e3

A sketch of the volume force acting on the particles is reported in Fig. 2. Particles move under the action of a body force, applied to mimic the action of a swirled flow dragging the particles, whose modulus and intensity is tuned to obtain a prescribed impact angle and velocity at the wall. The radial component of the force acting on the particles has been chosen to vary with a linear law according to the expression:

$$\mathbf{F}_{V,r} = m \omega^2 r \mathbf{i}_r \tag{10}$$

being ω the angular velocity of a rotating frame of reference with axis of rotation coincident with the cylinder axis, r the radial position of the particle and $\mathbf{i}_r$ the radial unit versor. The modulus of the tangential component is tuned by a constant according to:

$$\left|\mathbf{F}_{V,t}\right| = a \left|\mathbf{F}_{V,r}\right| \tag{11}$$

The constant a, together with the value of $|\mathbf{F}_{V,r}|$, determines the resulting initial spiral path and therefore the impact angle between the particles and the wall of the cylinder. The forces described by Eqs. (10) and (11) are added to the particles contact forces appearing in Eq. (3).

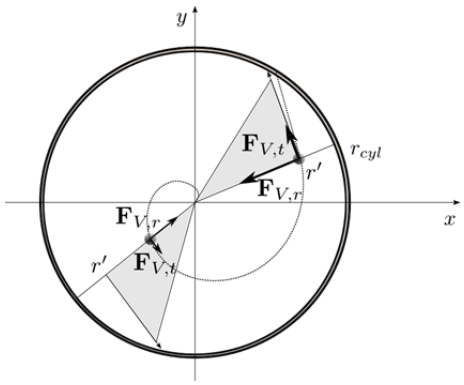

Figure 2. Volume forces acting on particles.

Particles immersed in a viscous flow are not expected to be affected by a strong drag when they are close enough to the wall to be well inside the boundary layer. Furthermore, when

particles accumulate onto the wall, the boundary layer shifts aside from the cylinder wall and almost no gas flow is allowed inside the particle layer if the packing level is high. The main actions exerted on the layer of deposited particles is that of the free flying particles impinging on the surface of the layer and that of the shear stress of the flow on the same surface. Thus, to mimic the absence of a drag force acting inside the particle layer, both radial and tangential components of the applied body force are vanished at a fixed radius $r' = r_{cyl} - \Delta$ from the centre of the cylinder, where Δ is properly assigned. If a perfect packing is realized, the thickness of the particle layer never reaches the region of application of the body force and all the energy initially gained by the particles is eventually dissipated by collisions. In this way, particles are subjected only to their inertia for $r' < r < r_{cyl}$. Such distance r_{cyl}, here set to 0.02 m, is chosen as a multiple of the particle diameter to have the establishment of a dense particle layer exchanging momentum with the layer of particles continuously energised by the body force acting in the core of the cylinder. The force intensity is selected by modifying the value of ω. In this work it is ω = 200 rad/s. The volume force acting on the particles is vanished at r' = 0.019 m from the centre of the cylinder, thus Δ = 0.001 m, i.e. ten particles diameters. No force component is applied along the cylinder axis direction.

Two different materials are used in the simulation for the particles and for solid walls, which are treated as granular walls. Particle–surface interaction can be described in terms of the stickiness of the particle and of the surface on which particles impinge [7]. Particle–particle and particle–surface stickiness is obtained tuning the friction contribution due to translational and rolling motion.

As suggested in [4,9], four cases have been considered by assuming limiting cases of prevalence of elastic or sticky interactions between particles and walls, as described in Section 1. For the NSP–NSW case, particles are assumed to be always rebounded by the surface; conversely, they are always trapped for SP–SW case. The SP–NSW and NSP–SW interactions are tuned by the mechanical properties of the particles and surface (slag). In this way, four possible limiting cases of interactions between particles and surface can be obtained as summarized in Table 1. To assign this behaviour to particles and wall, proper values of material properties are selected, as reported in Table 1. Properties without a subscript are related to both material *i* or material *j*, while those with double subscript (*i*,*j*) are related to the interaction between the materials *i*,*j* (i.e. the particle and the wall or conversely).

The choice of the time integration step Δt is constrained by the speed of the elastic energy transfer in the granular medium due to particle collisions, and to the particle overlap. According to the former argument, Δt has not to be large to avoid wrong energy transfer. Then the latter argument dictates that the overlap has not to be greater than $\delta = 0.5\, R_p$. For coal particles, the time integration step is set to $\Delta t = 10^{-8}$ s in the NSP–NSW, NSP–SW, SP–NSW regimes. While, to preserve the correct energy transfers in the SP–SW case, it is set equal to $\Delta t = 10^{-10}$ s.

4. RESULTS

Nondimensional quantities are defined by introducing the following reference variables [15]:

$$l^* = R_p \qquad , \qquad a^* = (1+a)\omega^2 r' \qquad , \qquad t^* = \sqrt{\frac{l^*}{a^*}} \tag{12}$$

With the assumed parameters, the reference time results to be $t^* = 0.0002$ s. The former equations lead to define the reference velocity as $u^* = \sqrt{2\omega^2 l^* R_p}$. Being $t_c = \pi\left(2k_n/m - \gamma_n^2/4\right)^{-1/2} = 10^{-6}$ s [14] the binary collision time among two particles estimated assuming that k_n and γ_n are computed from non-linear Hertz theory, the nondimensional collision time is $t_c/t^* = 0.005$. The external force is vanished at $r'/l^* = 95$.

Dynamics of Surface Coverage

Relevant results relative to particles segregation on the solid walls can be obtained inspecting a selected set of views of the considered geometry. Fig. 3 reports the time behaviour of K^*, the total particle kinetic energy for all the regimes simulated, normalized with respect to the maximum value of kinetic energy attained in the NSP–NSW case. When $r > r'$, particles are not under the action of the imposed volume force, thus they only move under the action of their inertia. Their kinetic energy attains a maximum value at about $t/t^* = 36$, immediately before the first impact with the cylinder walls, when the gained kinetic energy begins to be dissipated. In the NSP–NSW regime (typical of char particles impacting on a wall slag layer covered by other char particles), such value is less than one, being the maximum kinetic energy obtained later on, when the first impact of all the particles with the wall is fully developed. Such evidence can be explained in terms of the non sticky particle nature. Indeed, if NSPs collide, their kinetic energy is almost conserved during the collision. Hence, after a binary collision, particles depart from each other. When a particle hits the NSW, the kinetic energy is still almost conserved and, after the rebound, the particle moves towards the region of non-vanishing volume force. For a while, both particles approaching the walls and rebounded particles are subject to the volume force and so they continue to gain kinetic energy. The maximum value of the kinetic energy is attained at $t/t^* = 48$. After this period, as the particles near the surface are trapped by the incoming ones, the majority of particles fly close to the wall. The dissipation of the collisions increases due to a greater number of collisions in such a dense layer. Then, the kinetic energy is reduced towards an equilibrium value that establishes between the energy transmitted by the particles still flying in the region of active volume force and the energy dissipated. Conversely, when SP particles collide (SP–NSW regime, typical of molten ash or highly-converted char particles impacting on a wall slag layer covered by char particles), their kinetic energy is partially converted into plastic deformation and it rapidly dissipates due to the low value of the restitution coefficient (it is recalled that in this work $\varepsilon = 0.9$ is characteristic of a non sticky behaviour, while $\varepsilon = 0.1$ of a sticky one). Moreover, the torque due to the rolling friction linked to particle contacts reduces even further the particles velocity. In this case, granular cohesion is able to cluster the particles, resulting in coarser grains having a larger inertia.

The effect of a sticky wall is more complex. When sticky particles hit the sticky wall (SP–SW regime, typical of molten ash or highly-converted char particles impacting on a wall slag layer), almost all the kinetic energy is dissipated, and therefore the curve presents a monotonic decreasing behaviour after the first impact of the particles on the wall. When non sticky particles hit a sticky wall (NSP–SW regime, typical of char particles impacting on a wall slag layer), the dynamics is completely different: the kinetic energy firstly decreases but successively returns to increase to a level comparable to that gained before the first impact. To explain this behaviour it is important to observe that the first particles impinging the wall are trapped forming a new layer able to behave as a non sticky wall. However, this layer differs from a flat non sticky wall because of the irregular distribution of the lying particles, making it essentially a corrugated non sticky wall.

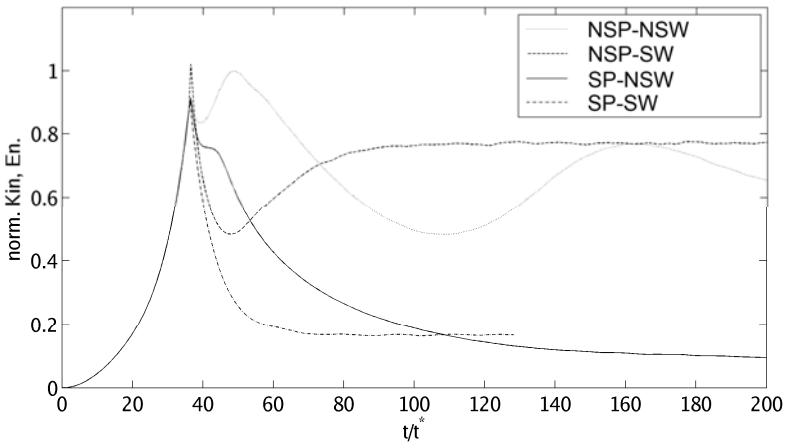

Figure 3. Time behaviour of normalized kinetic energy versus nondimensional time.

Fig. 4 shows the top view of the particles inside the cylinder for NSP–NSW (left) and NSP–SW (right) case at $t/t^* = 100$ ($t = 0.02$ s). Two features are clearly highlighted. Firstly, the thickness of the dense layer is much larger in the case of a sticky wall, meaning that, being the total number of particles the same, a higher void fraction characterizes this case. Secondly, observing the colouring that represents the velocity magnitude, a larger velocity distribution is detected in the case of a sticky wall, that spans from zero at the wall, due to adherence, to about 12 m/s for particles located in the outer region (with respect to the wall). In the case of a non sticky wall, particles are able to slide even at the wall, making possible reciprocal movements that in turn allow to reach a higher packing degree.

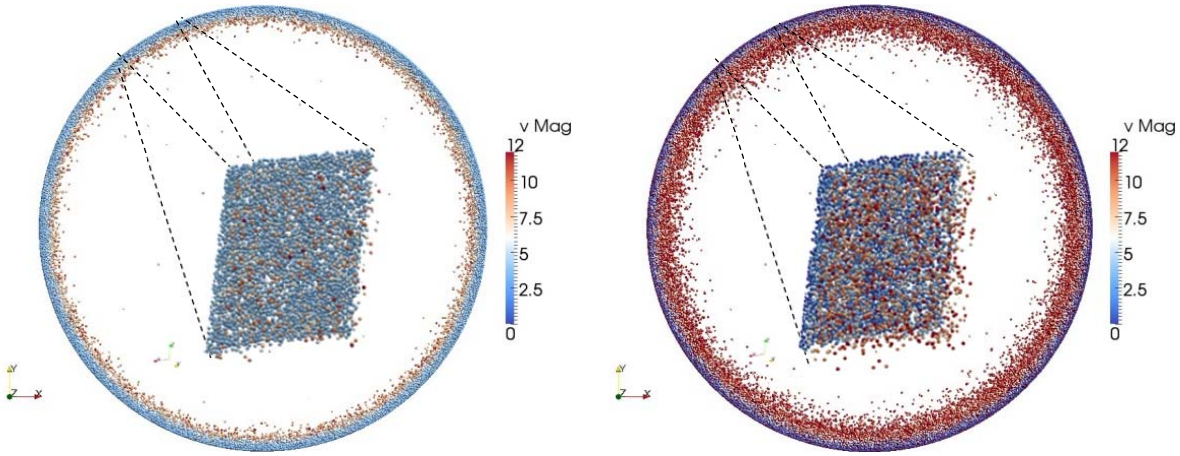

Figure 4. Top view of particle positions at $t/t^* = 100$ ($t = 0.02$ s). Left: NSP–NSW, right: NSP–SW. The inset shows the perspective view of a small portion of the particle layer near the lateral cylinder surface. Colouring is for the velocity magnitude (m/s).

The following dynamics can be recognized: the particles that first impinge the surface are rebounded and move towards the region of non-vanishing forces. During this back-motion, they collide with the other incoming particles and are redirected once again towards the wall, becoming trapped. Even if trapped, they are still free to rotate being the wall non sticky, under the action of the torque exerted by the neighbour particles. This capability allows incoming particles to accommodate in the layer formed on the wall by plunging into the neighbouring ones. If the wall is sticky, particles that firstly collide with the cylinder walls are not

rebounded and adhere to the wall, Fig. 4, right. In this case, when the incoming particles collide with the adhered particles layer, they are rebounded and their kinetic energy is transferred to the particles immediately lying on the wall, where it is dissipated. In this latter case the possibility of an incoming particle to accommodate on the wall by plunging into the other particles is hindered, while a non-uniform particle distribution near the wall is promoted. As a result, the number of particles which are redirected to the non-vanishing force region is increased. These considerations result in the establishment of a particle layer characterized by a different particle spatial distribution between the two considered cases.

The results concerning the SP–NSW and SP–SW regimes are reported in Fig. 5, left and right, respectively (t = 0.02 s). In the SP–NSW case, when particles collide, the cohesion forces allow for particles to create coarser grains while moving towards the wall. It is worth noting that the SP–NSW regime realizes the most uniform spatial deposition of particles on the walls. Such evidence is confirmed by the inspection of the inset in Fig. 5 (left). It is clearly shown that the number of particles floating in the non-vanishing force region is drastically reduced. This is the unique case in which only two to three layers of superimposed particles almost form near the cylinder walls. Equally, the superficial void fraction in the SP–NSW case is lower than in any other case. Hence, it can be argued that for the SP–NSW regime a full coverage of the lateral surface of the cylinder is promoted.

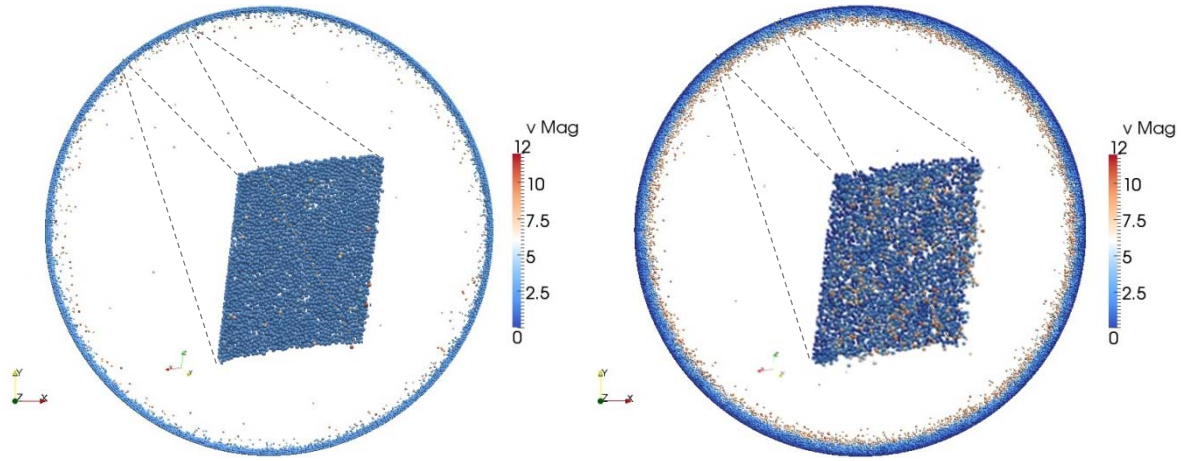

Figure 5. Top view of particles positions at t/t^* = 100 (t = 0.02 s). Left: SP–NSW, right: SP–SW. The inset shows the perspective view of a small portion of the particle layer near the lateral cylinder surface. Colouring is for the velocity magnitude (m/s).

Fig. 5, right, illustrates the SP–SW case. The wall stickiness promotes the formation of non-uniform clusters of particles near the surface. In this case, the formation of a thin layer of superposed particles on the cylindrical wall is anymore allowed, but the particle deposition is more uniform compared to the NSP–SW case. A possible explanation can be given by considering that the particle stickiness acts by forming coarser grains having greater mass, and then a higher inertia. Hence, when collisions occur, they are able to displace the formerly adhered particles giving them the possibility to plunge into the formed layer.

Analysis of Results in Fully Developed Conditions

Fig. 3 shows that for the cases with included stickiness, a fully developed flow regime seems to be rapidly attained or approaching at t/t^* = 200. Here it is defined a flow as fully developed when equilibrium is established between the kinetic energy dissipated by collisions and the

kinetic energy added to the particles by the action of the body force. At this time, the NSP–NSW regime was still unable to reach a perfectly steady equilibrium condition, while the SP–NSW regime appeared close to fully developed conditions. These simulations were therefore continued to determine the time required to reach the fully developed equilibrium regime.

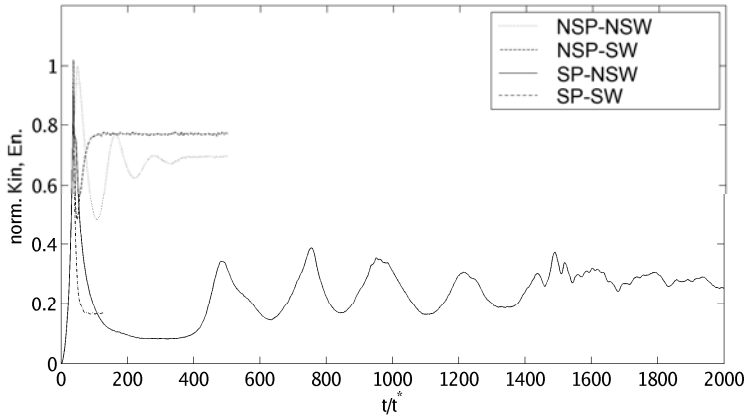

Figure 6. Time behaviour of normalized kinetic energy versus nondimensional time, from 0 to 2000.

The complete computed transient of the global particle kinetic energy is reported in Fig. 6. Such picture clearly shows that the NSP–NSW and SP–NSW cases cannot be considered in equilibrium at time $t/t^* \approx 100$. Furthermore, the time behaviour of the kinetic energy for these last two regimes is quite different: the system of particles globally behaves as a spring–mass–damper, but the normalized energy attains different constant mean values at different times, about $K^* = 0.18$ and $t/t^* = 80$ for SP–SW, $K^* = 0.77$ and $t/t^* = 120$ for NSP–SW, $K^* = 0.71$ and $t/t^* = 400$ for NSP–NSW, K^* approx. 0.27 and $t/t^* > 2000$ for SP–NSW, which is the last time step performed in this simulation. Two different levels of equilibrium kinetic energy are then obtained, low and high. Low K^* corresponds to cases with sticky particles, with the lower when the wall is sticky, too. High K^* is relevant to non sticky particles, but the wall stickiness increases the K^* equilibrium level.

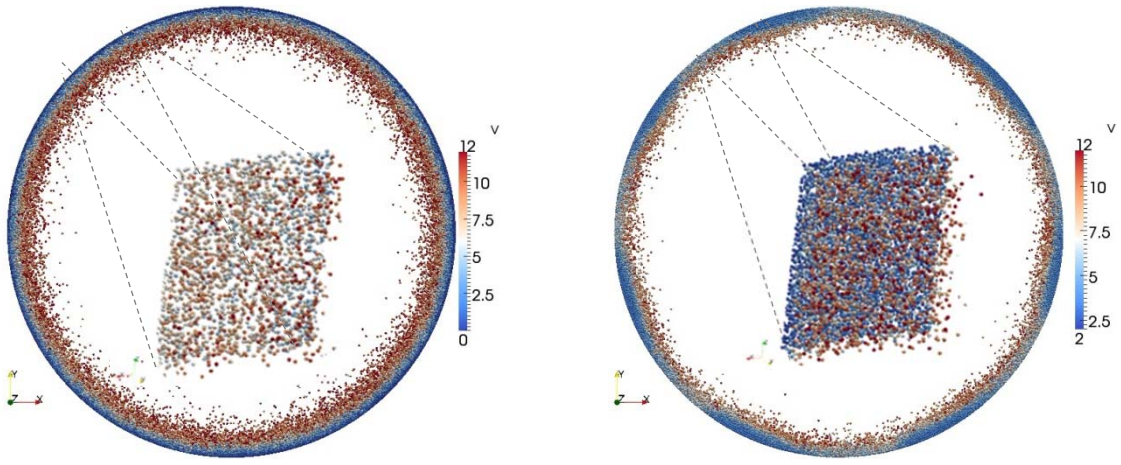

Figure 7. Instantaneous view of the *xy* plane particle positions at fully developed conditions. Left: NSP–NSW, right: NSP–SW. Colouring is for the velocity magnitude (m/s).

The structure of the layer of particles at the fully developed state for the different cases helps to explain the observed behaviour. It is reported in Figs. 7 and 8, in a similar fashion as done

in Figs. 4 and 5 for $t/t^* = 100$. Observing the structure of the layer it is possible to distinguish the key parameters affecting the established equilibrium. While the absence of sticky effect is favourable for the conservation of energy, the effect of the body force depends on the number of particles that float away from the wall. Therefore, even if less energy is dissipated in the NSP–NSW regime, particles spread on a much thicker layer with large velocity differences. Compared to the NSP–SW case, it results that the first particles that adhere to the wall form a thin layer able to rebound the subsequent arriving particles without the possibility to displace. In other words, the last case corresponds to the formation of a single layer of particles exchanging moment, while the former corresponds to the segregation of particles inside and outside the region of acting body force with low momentum exchange. Particles stickiness changes the behaviour of these interactions, leading to the establishment of equilibrium levels with lower intensity of the kinetic energy. Now the main mechanism appears to reside in the ability of clusters of particles to increase and survive to successive collisions. This clearly occurs in the SP–NSW regime, where large irregular structures form and are able to slide on the wall, making very difficult to reach an equilibrium state.

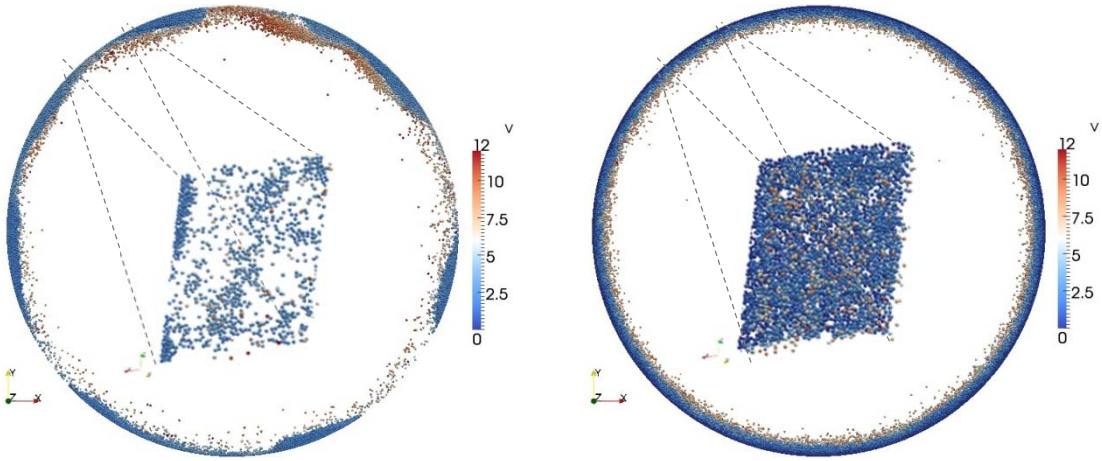

Figure 8. Instantaneous view of the *xy* plane particle positions at fully developed conditions. Left: SP–NSW, right: SP–SW. Colouring is for the velocity magnitude (m/s).

5. CONCLUSIONS

The results collected represent an initial assessment of the different regimes that can establish when particles impinge on walls with a trajectory that mimics the action of swirling flows, as those typically induced to coal particles in an entrained-flow gasifier. Depending on several parameters, as a function of the degree of particles conversion and slag viscosity, very different behaviours of the accumulating particles near the walls can be observed. A first effect regards the resulting residence time of the particles in the gasifier. A second is connected to the particle concentration and exchange of both solid and gas phase with the outer layers, expected to be beneficial for a complete conversion of the carbon. The proposed simulations represent a first attempt to get a detailed observation of the establishing structures, at least in the limiting regimes that can be described with the assumptions here adopted. By considering different regimes (char or molten ash particles impacting on the wall slag layer, that in turn can be either accessible or covered by unconverted char particles), conditions able to promote very early particle segregation in the near-wall region are identified. Work is on-going to establish more quantitative assessments of the regimes here observed by varying the several parameters expected to play a significant role, like the velocity and the angle of impact with the wall, the restitution coefficients, the cohesion forces

and the particle size distribution, and to include a full description of the gas phase–solid phase interaction.

ACKNOWLEDGEMENTS

The support of ADP MiSE/CNR, Project “Carbone Pulito”, is gratefully acknowledged.

REFERENCES

1. Shimizu, T. and Tominaga, H. (2006). A model of char capture by molten slag surface under high-temperature gasification conditions. *Fuel*, **85**, 170–178.
2. Ni, J., Yu, G., Guo, Q., Zhou, Z. and Wang, F. (2011). Submodel for predicting slag deposition formation in slagging gasification systems. *Energy Fuels*, **25**, 1004–1009.
3. Li, S. and Whitty, K.J. (2012). Physical phenomena of char–slag transition in pulverized coal gasification. *Fuel Process. Technol.*, **95**, 127–136.
4. Chen, L. and Ghoniem, A.F. (2013). Development of a three-dimensional computational slag flow model for coal combustion and gasification. *Fuel*, **113**, 357–366.
5. Montagnaro, F. and Salatino, P. (2010). Analysis of char–slag interaction and near-wall particle segregation in entrained-flow gasification of coal. *Combust. Flame*, **157**, 874–883.
6. Montagnaro, F., Brachi, P. and Salatino, P. (2011). Char–wall interaction and properties of slag waste in entrained-flow gasification of coal. *Energy Fuels*, **25**, 3671–3677.
7. Ambrosino, F., Aprovitola, A., Brachi, P., Marra, F.S., Montagnaro, F. and Salatino, P. (2012). Investigation of char–slag interaction regimes in entrained-flow gasifiers: linking experiments with numerical simulations. *Combust. Sci. Technol.*, **184**, 871–887.
8. Ambrosino, F., Aprovitola, A., Brachi, P., Marra, F.S., Montagnaro, F. and Salatino, P. (2013). Entrained-flow gasification of coal under slagging conditions: relevance of fuel–wall interaction and char segregation to the properties of solid wastes. *Fuel*, **114**, 44–55.
9. Troiano, M., Carbone, R., Montagnaro, F., Salatino, P. and Solimene, R. (2014). A lab-scale cold flow model reactor to investigate near-wall particle segregation relevant to entrained-flow slagging coal gasifiers. *Fuel*, **117**, 1267–1273.
10. Cundall, P.A. and Strack, O.D.L. (1979). A discrete numerical model for granular assemblies. *Géotechnique*, **29**, 47–65.
11. Zhou, Z., Kuang, S., Chu, K. and Yu, A. (2010). Discrete particle simulation of particle–fluid flow: model formulations and their applicability. *J. Fluid Mech*., **661**, 482–510.
12. Campbell, C.S. (2006). Granular material flows – an overview. *Powder Technol.*, **162**, 208–229.
13. Kloss, C., Goniva, C., Hager, A., Amberger, S. and Pirker, S. (2012). Models, algorithms and validation for opensource DEM and CFD–DEM. *Prog. Comput. Fluid Dyn.*, **12**, 140–152.
14. Silbert, L. E., Ertaş, D., Grest, G. S., Halsey, T. C., Levine, D., Plimpton, S. J. (2001). Granular flow down an inclined plane: Bagnold scaling and rheology, *Phys. Rev. E*, **64**, 051302.
15. Kumaran, V. and Maheshwari, S. (2012). Transition due to base roughness in a dense granular flow down an inclined plane. *Phys. Fluids,* **24**, 053302.